NANO LETTERS

Letter

pubs.acs.org/NanoLett

Perfect Thermal Emission by Nanoscale Transmission Line Resonators

Baoan Liu, Wei Gong, Bowen Yu, Pengfei Li, and Sheng Shen*

Department of Mechanical Engineering, Carnegie Mellon University, Pittsburgh, Pennsylvania 15213, United States

Supporting Information

ABSTRACT: Thermal radiation with a narrow-band emission spectrum is of great importance in a variety of applications such as infrared sensing, thermophotovoltaics, radiation cooling, and thermal circuits. Although resonant nanophotonic structures such as metamaterials and nanocavities have been demonstrated to achieve the narrow-band thermal emission, maximizing their radiation power toward perfect emission still remains challenging. Here, based on the recently developed quasi-normal mode theory, we prove that thermal emission from a nanoscale transmission line resonator can always be maximized by tuning the waveguiding loss of the resonator or bending the structure. By use of nanoscale transmission line resonators as basic building blocks, we experimentally demonstrate a new type of macroscopic perfect and tunable thermal emitters. Our experimental demonstration in conjunction with the general theoretical framework from the quasi-normal mode theory lays the foundation for designing tunable narrow-band thermal emitters with applications in thermal infrared light sources, thermal management, and infrared sensing and imaging.

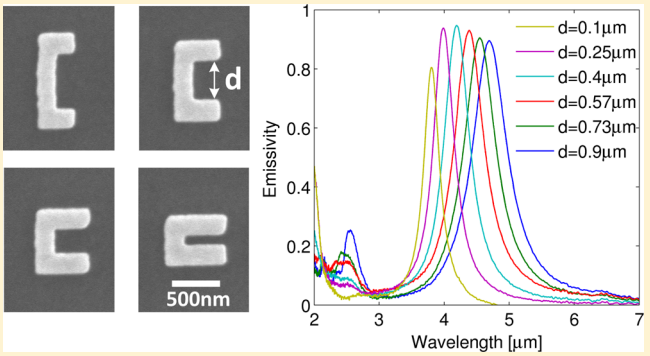

KEYWORDS: *Thermal radiation, perfect emitter, transmission line, optical resonator, quasi-normal mode*

Although thermal radiation usually has a fairly broad spectrum, the narrow-band control of thermal emission is of great importance in a variety of applications such as infrared sensing,[1] thermophotovoltaics,[2,3] radiation cooling,[4] and thermal circuits.[5,6] One popular method for achieving narrow-band thermal emission is to tailor the radiation spectra of resonant nanophotonic structures like metamaterials, nanocavities, and so on.[7,8] The corresponding peak frequencies of thermal radiation can readily be tuned by modifying the geometries of the nanophotonic structures. However, a long-standing but critical challenge for designing thermally driven nanophotonic resonators is how to further maximize their narrow-band thermal radiation toward "perfect" emission, where the emissive power at the peak frequency reaches the blackbody radiation limit in the far-field. For instance, in order to maximize the thermal emission from a metamaterial, impedance matching based on simplified electrical circuit models is widely used.[7,9,10] Yet, because the electric and magnetic responses of "meta-atoms" are generally correlated with each other in a complicated manner, what is lacking is a general theoretical framework that allows one to understand and design the thermal radiation from a metamaterial or an arbitrary resonant structure in a more direct and quantitative way.

In this work, we employ nanoscale transmission line resonators as fundamental building blocks to create a new type of perfect thermal emitters. Transmission lines are essentially the waveguides composed of one or multiple metallic wires. They were invented more than a century ago[11] and extensively applied for radio frequency communications. It was discovered that microscale transmission lines could efficiently guide terahertz and infrared waves with highly confined waveguiding modes.[12−14] On the basis of the recently developed quasi-normal mode theory,[15] we prove that thermal emission from a nanoscale transmission line resonator can always be maximized by tuning the waveguiding loss of the resonator or bending the structure. With the maximized thermal radiation from an individual resonator, we experimentally demonstrate macroscopic perfect thermal emitters constructed by nanoscale transmission line resonator arrays. The perfect narrow-band thermal emitters based on transmission line resonators are particularly promising for low-power narrow-band infrared sources, where the infrared transmission line structures can be fabricated by using large-scale techniques such as nanoimprinting,[16] chemical synthesis,[17] and so forth, and their emission can be easily tuned to cover the entire infrared spectrum by changing their geometries.

Thermal Emission from a Single Nanoscale Transmission Line Resonator. Due to the modulation of the resonant mode in the infrared range, thermal emission from an optical resonator can be enormously enhanced at the resonant

Received: August 27, 2016
Revised: December 30, 2016
Published: January 3, 2017

DOI: 10.1021/acs.nanolett.6b03616
Nano Lett. 2017, 17, 666−672

frequency, leading to a narrow-band emission spectrum, as described by the Purcell effect.[18] Furthermore, the spectral emission power from a nanoscale optical resonator, particularly at the resonant frequency, can exceed Planck's law for blackbody radiation in its physical area. In this case, the corresponding radiation cross-section area of the resonator $A_r = \frac{\phi(\omega)}{\phi_B(\omega)}$ is much larger than its physical area A_p, where $\phi(\omega)$ is the thermal emission power of the resonator, and $\phi_B(\omega) = \frac{\Theta(\omega, T)}{2\pi}\left(\frac{8\pi^3 c_0^2}{\omega^2}\right)$ indicates the energy flux of blackbody radiation. As a result, a perfect macroscopic thermal emitter can be created by packing the nanoscale super-Planckian optical resonators on a surface, as shown in Figure 1. However, in order to maintain the resonant mode of each resonator undisturbed, the separation between two adjacent resonators needs to be large enough to prevent any strong interaction among the resonators. Hence, maximizing the thermal emission of a single resonator $\phi(\omega)$ to enable a large radiation cross-section area A_r is the key.

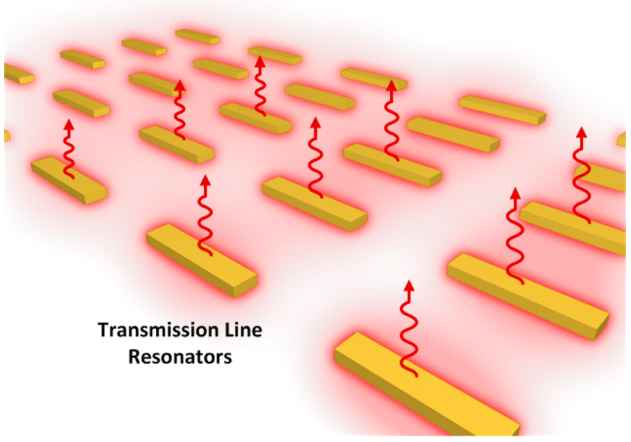

Figure 1. Schematic of a macroscopic thermal emitter made by optical resonator arrays.

Thermal radiation from an optical resonator has been poorly understood, especially when its dimension is at the nanoscale, which is much smaller than the wavelength of thermal radiation defined by Wien's displacement law. There exists no general theory for directly designing optical resonator based thermal emitters. The widely used model of equating absorptivity to emissivity becomes invalid for nanoscale resonant thermal emitters.[19] This is because the "emissivity" and "absorptivity" of a nanoscale emitter are difficult to be defined due to the super-Planckian radiation and the fact that the absorption cross-section can significantly exceed the physical area of the nanocale emitter.[20] Thermal emission from an optical resonator accounts for the emitted light in all directions and with all polarizations, whereas the optical absorption strongly depends on the direction and polarization of the incident light. Moreover, the well-known Purcell effect only captures the optical cavity behavior but ignores the dissipative properties of a thermal emitter.[18] Therefore, thermal radiation from an optical resonator cannot be designed by following the conventional rule for optical resonators or cavities, that is, enhancing the quality factor while simultaneously reducing the mode volume. We derive a new formalism to elucidate the thermal radiation from an arbitrary optical resonator based on the quasi-normal mode theory and fluctuational electrodynamics.[15] For an arbitrary emitter, the thermal emission power density $\phi(\omega)$ can be formulated in terms of the dyadic Green's function $G_{\omega,r,r'}$ and fluctuational electrodynamics as

$$\phi(\omega) = \frac{\Theta(\omega, T)}{2\pi} 4\omega\mu_0 \{\mathrm{Tr}[\int_V \mathrm{d}r^3 \sigma \mathrm{Im}[G_{\omega,r,r}]] - \omega\mu_0 \mathrm{Tr}[\int_V \mathrm{d}r^3 \int_V \mathrm{d}r'^3 \sigma^2 G^*_{\omega,r,r'} \cdot G_{\omega,r,r'}]\} \quad (1)$$

where $\Theta(\omega, T) = \hbar\omega/[\exp(\hbar\omega/k_B T) - 1]$ is the Planck's distribution, $\sigma = \omega\,\mathrm{Im}[\epsilon]$ indicates the electric conductivity of the emitter V, and μ_0 denotes the vacuum permeability. According to the quasi-normal mode theory, the dyadic Green's function $G_{\omega,r,r'}$ for a resonant thermal emitter can be expanded by the resonant mode $[E_0(r), H_0(r)]$ near the resonant frequency ω_0 as[21]

$$G_{\omega,r,r'} \approx \frac{E_0(r) \cdot E_0^*(r')}{\omega\mu_0(\omega_0 - \omega)N} \quad (2)$$

where $[E_0(r), H_0(r)]$ are the eigen-solution of the source-free Maxwell equations satisfying $\nabla \times E_0(r) = i\omega_0\mu_0 H_0(r)$ and $\nabla \times H_0(r) = -i\omega_0\epsilon(r)E_0(r)$, and $N = \int_\infty \mathrm{d}r^3 \left[\frac{\partial\omega\epsilon}{\partial\omega}(\omega_0)E_0^2 - \frac{\partial\omega\mu_0}{\partial\omega}H_0^2\right]$ is the normalization factor of the resonant mode. Substituting eq 2 into eq 1, we derive that the thermal emission spectrum of a resonant

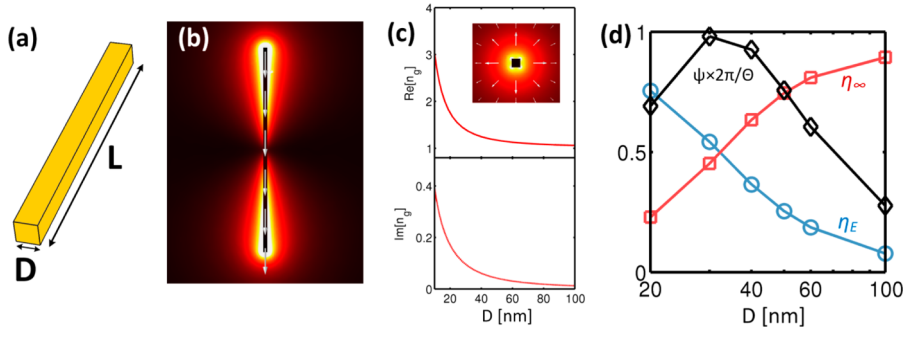

Figure 2. Tuning the dissipative mode loss of a straight transmission line resonator. (a) Schematic of the transmission line resonator. (b) Electric field profile of the fundamental resonant mode. Arrows indicate the electric field polarization directions. (c) Effective propagating index of the transmission line waveguiding mode at the wavelength of 7 μm, inset: the electric field profile of the waveguiding mode. (d) Fractional mode losses η_E and η_∞, and the thermal emission peak ψ for the cases with different D.

DOI: 10.1021/acs.nanolett.6b03616
Nano Lett. 2017, 17, 666−672

thermal emitter follows a Lorentz line-shape, where the peak $\psi = \phi(\omega_0)$ equals

$$\psi = \frac{\Theta(\omega_0, T)}{2\pi} 4\eta_E \eta_\infty \tag{3}$$

In eq 3, η_E and η_∞ are the dissipative and radiative fractional mode losses, respectively, which can be expressed purely by the resonant mode field profile $[E_0(r), H_0(r)]$ (See Methods). For the optical resonators whose resonant modes have quasi-static electric field profile, η_E and η_∞ satisfies $\eta_E + \eta_\infty \approx 1$,[15] which can be understood as the percentage of the mode energy lost inside the resonator and to the far-field free space, respectively. As a result, the upper limit of ψ equals $\frac{\Theta}{2\pi}$ when the dissipative and radiative mode losses are matched, that is, $\eta_E = \eta_\infty = 0.5$. It thus defines the limit of the radiation cross-section due to a single resonant mode, which equals $A_r = \lambda^2/2\pi$, where $\lambda = 2\pi\omega/c_0$ is the free-space wavelength. Equation 3 further suggests that the distance between nanoscale optical resonators when forming a macroscopic emitting surface cannot be too small, otherwise ψ can be severely deteriorated due to the significant increase of the dissipative mode loss η_E to neighboring resonators.

By scrutinizing their resonant modes using the quasi-normal mode formulation, we introduce two general principles to respectively tune the dissipative and radiative mode losses (η_E and η_∞) of transmission line resonators toward the maximized thermal emission. Consider a simple transmission line resonator made from a gold nanowire with a square shape cross section, as shown in Figure 2a. The length of the nanowire $L = 2.5$ μm, and the lateral size $D = 40$ nm. The electric field profile of its fundamental resonant mode $[E_0(r), H_0(r)]$ can be directly calculated by using the finite-element method,[22] as plotted in Figure 2b. Figure 2b clearly shows the Fabry–Perot-like resonance of the transmission line modes guided along the gold nanowire, where the resonant wavelength equals $\lambda_0 = 7$ μm $\approx 2L \times \mathrm{Re}[n_g]$ and n_g is the propagating index of the waveguide. In addition, the electric field is highly confined in the gold nanowire. In Figure 2c, we simulate the propagating index n_g of the gold nanowire transmission lines with different values of D, where the waveguiding loss characterized by $\mathrm{Im}[n_g]$ monotonically increases as the value of D decreases. We then adopt the quasi-normal mode theory to evaluate the fractional mode losses η_E and η_∞ and the thermal emission peak value ψ of the transmission line resonators at the same length $L = 2.5$ μm but with different values of D. As shown in Figure 2d, η_E is monotonically increasing with shrinking values of D, which follows the same trend of the waveguiding loss in Figure 2c. At $D \sim 40$ nm, the dissipative mode loss and the radiative mode loss are matched, that is, $\eta_E = \eta_\infty \approx 0.5$, and the peak of the thermal emission spectrum reaches the maximum $\psi \to \frac{\Theta}{2\pi}$. Thus, tuning the waveguide losses by modifying the transverse size of transmission line resonators serves as a general principle to tune the dissipative mode loss η_E.

To tune the radiative mode loss η_∞, we consider two types of bended transmission line resonators, C-shape and V-shape, as shown in Figure 3a,b respectively. In both the cases, the length and the lateral dimension of the transmission lines are fixed to be $L = 2.5$ μm and $D = 50$ nm. Figure 3c,d plots the fractional mode losses η_E and η_∞ and the peak height ψ for the C-shape cases with different gap distances d and the V-shape cases with

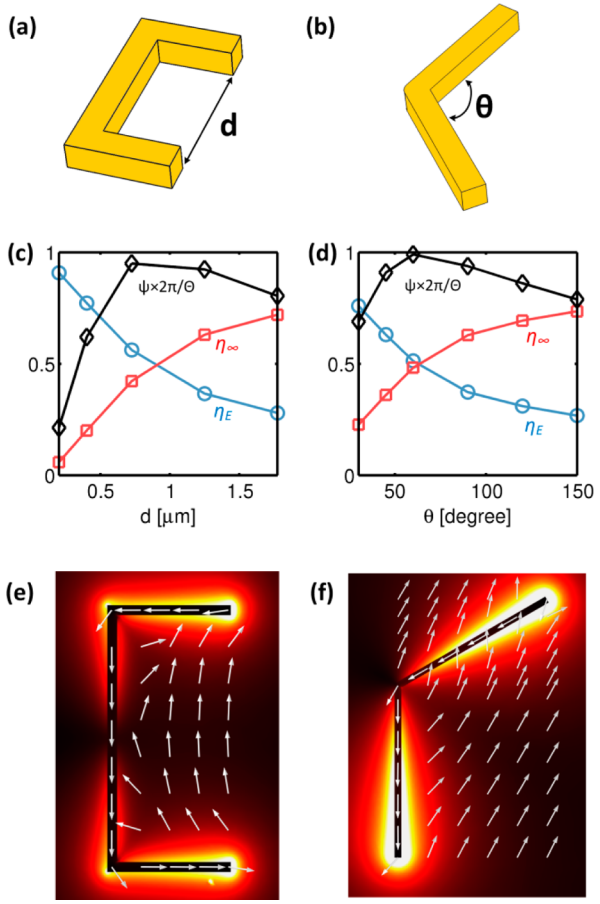

Figure 3. Tuning the radiative mode loss of a bended transmission line resonator. (a,b) Schematics of the C-shape and V-shape transmission line resonators. (c,d) Fractional mode losses η_E and η_∞, and the thermal emission peak ψ of the cases with different d and θ. (e,f) Electric field profiles of the fundamental resonant modes for both the cases. Arrows indicate the electric field polarization directions.

different bending angles θ. In both the cases, η_∞ monotonically decreases as d for the C-shape resonator and θ for the V-shape resonator are reduced. At certain values of d and θ, η_∞ is equal to η_E, and the thermal emission peak ψ reaches the maximum. To reveal the mechanism of tuning the radiative mode loss by bending the transmission line resonator, we rearrange the definition of the resonant mode $[E_0(r), H_0(r)]$ as

$$\begin{aligned} \nabla \times E_0(r) &= i\omega_0\mu_0 H_0(r) \\ \nabla \times H_0(r) &= -i\omega_0\epsilon_0 E_0(r) - i\omega_0 P(r) \end{aligned} \tag{4}$$

where $P(r) = [\epsilon(\omega_0, r) - \epsilon_0]\, E_0(r)$ indicates the induced electric dipole moments inside the emitter. Because the fundamental resonant mode confines the fields in a subwavelength scale, $E_0 = \omega_0^2\mu_0 \int_{V_E} dr'^3 [G_{\omega_0 r r'} \cdot P(r')] \approx \omega_0^2\mu_0 G_{\omega, r, r_0} \int_{V_E} dr'^3 P(r')$ when $|r_0 - r'| \ll \lambda$. Therefore, $[E_0, H_0]$ can be interpreted as the field emitted by an equivalent dipole located at r_0 with the dipole moment $\int_{V_E} dr^3 P(r)$. Because η_∞ is proportional to $\int_{\partial V} \frac{1}{2} \mathrm{Re}[E_0 \times H_0^*]$, that is, the total outward energy flux from an enclosure surface ∂V. It has $\eta_\infty \propto |\int_{V_E} dr^3 P(r)|^2$ according to the property of dipole radiation.[23] As a result, by bending the transmission line resonator without changing its resonant mode, the radiative mode loss η_∞ can be

DOI: 10.1021/acs.nanolett.6b03616
Nano Lett. 2017, 17, 666–672

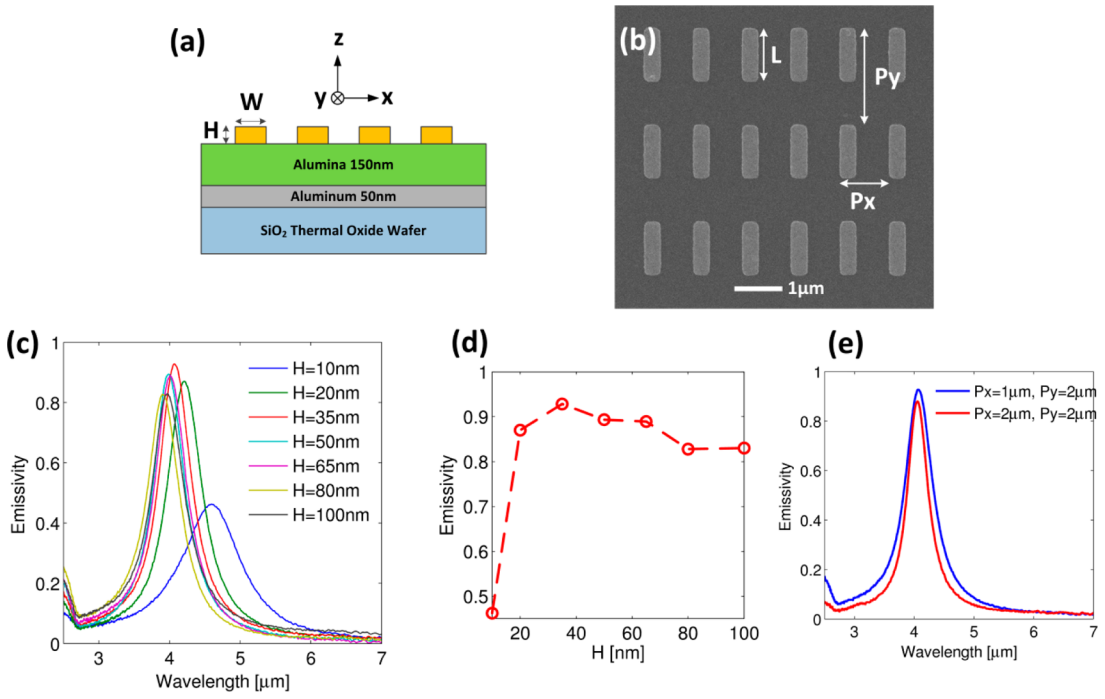

Figure 4. Emissivity of straight transmission line resonator arrays. (a) Schematic of the cross section of the transmission line resonator arrays. (b) SEM image of the top view of the transmission line resonator arrays. (c) Experimentally measured *y*-polarized emissivity spectra of the arrays with different H and (d) their corresponding peak values. The Q-factor for the case with H = 35 nm equals 7.3. (e) Experimentally measured *y*-polarized emissivity spectra of the resonator arrays for H = 35 nm with different periodicities.

tuned because it introduces a directional vector $\hat{\mathbf{e}}(r)$ in the integral $\eta_\infty \propto |\int_{V_E} dr^3 \hat{\mathbf{e}}(r) \cdot P(r)|^2$. For both C-shape and V-shape transmission line resonators, the electric fields inside the metal wires are all polarized along the wires, as shown in Figure 3e,f. Therefore, bending the structure can efficiently reduce the overall equivalent dipole moment $\int_{V_E} dr^3 P(r)$ in both the cases, and η_∞ can be decreased accordingly.

Perfect Macroscopic Thermal Emitter Composed of Nanoscale Transmission Line Resonators. On the basis of the aforementioned principles, we experimentally investigate the thermal radiation from transmission line resonator arrays. Because the thermal emission from each resonator usually emits in all directions, the substrate is chosen to be a metal plate with a dielectric spacer (as illustrated in Figure 4a), where the metal plate performs as a mirror to reflect all the radiation to the upper space. We demonstrate that perfect thermal emission of the resonator arrays can always be approached by either tuning the thickness H of the metal wires or bending the individual structure, as shown in Figures 2 and 3. To prove the concept, all of the transmission line resonators in our experiment are aligned in the *y*-direction, indicating the maximized emissivity at the *y*-polarization. The samples are fabricated using standard electron beam (E-beam) lithography techniques (see Methods). The scanning electron microscope (SEM) image of transmission line resonators is shown in Figure 4b.

The thermal emissivity spectra of the samples are characterized in the wavelength range of 2−12 μm. The emissivity is evaluated as the absorptivity according to Kirchhoff's law. This law is fully applicable in our experiment because the size of the arrays is much larger than the characteristic wavelength of thermal radiation. Because our samples are opaque, we directly measure their reflectivity. The emissivity can then be calculated by one minus the reflectivity. To obtain the reflectivity, the *y*-polarized reflectivity spectra of the samples are measured by a Fourier-transform infrared (FTIR) spectrometer combined with an infrared microscope. An infrared linear polarizer is used in the infrared microscope, which only allows the *y*-polarized reflected light to pass through. The reflection spectra of the samples are normalized to that of a gold standard mirror.

Figure 4c plots the measured emissivity spectra of the resonator arrays (L = 1 μm and W = 0.25 μm) for different H. The period of the arrays are chosen to be P_x = 1 μm and P_y = 2 μm in order to satisfy $A_r \leq P_x P_y < \lambda^2/\pi$ and reach the blackbody limit at the peak of $\lambda \sim 4$ μm while preventing the strong interactions between adjacent resonators. The narrow-band thermal emission is observed for all the cases, where the peak wavelength corresponds to the resonance wavelength of the fundamental Fabry−Perot type mode, that is, $\lambda_0 \sim 2Ln_g$. We also plot the peak values as a function of H in Figure 4d. By reducing H, the emissivity peak first increases and then decreases. At the optimized thickness H = 35 nm, the emissivity peak reaches the maximum. Comparing with the previous designs of perfect narrow-band thermal emitters based on grating,[24] metamaterials,[7] and photonics crystals,[25] our measured maximum emissivity (0.95) is very close to the state-of-the-art (0.97).[1,7] The discrepancy between the maximum peak value and the blackbody limit (100% emissivity) is mainly attributed to the nonresonance components of the radiation field, which are also known as the background noise in the expansion of dyadic Green's function in eq 2.[21] In the context of our aforementioned quasi-normal mode theory, its impact to thermal radiation is omitted. The other reason for the discrepancy is the limited resolution of our data points. The variation of the emissivity peaks in Figure 4d agrees well with the theoretical investigation in Figure 2c. Moreover, this narrow-band emissivity is not due to the strong

DOI: 10.1021/acs.nanolett.6b03616
Nano Lett. 2017, 17, 666−672

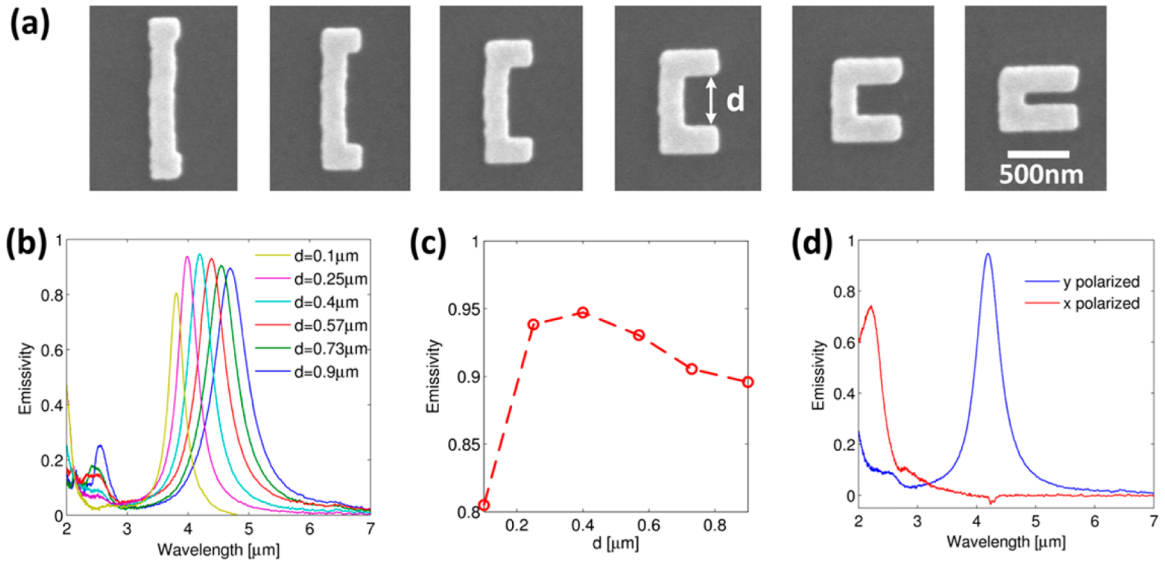

Figure 5. Emissivity of C-shape transmission line resonator arrays. (a) SEM images of the C-shape transmission line resonators with different gap distances d. (b) Experimentally measured y-polarized emissivity spectra of the C-shape resonator arrays with different d, and (c) the corresponding peak values. (d) Experimentally measured y-polarized and x-polarized emissivity spectra of the C-shape arrays with d = 400 nm.

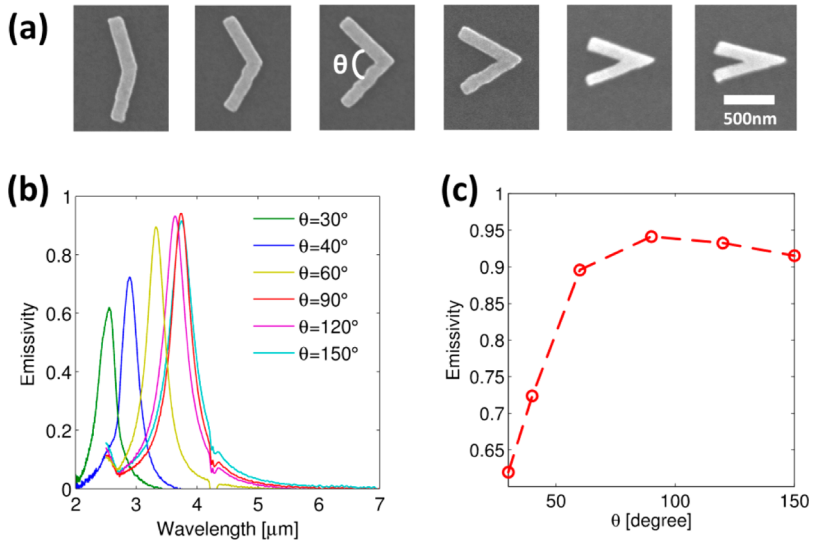

Figure 6. Emissivity of V-shape transmission line resonator arrays. (a) SEM images of the V-shape transmission line resonators with different bending angles θ. (b) Experimentally measured y-polarized emissivity spectra of the V-shape resonator arrays with different θ and (c) the corresponding peak values.

interactions among resonators (e.g., grating effect). In Figure 4e, the emissivity spectra of the resonator arrays with different P_x and P_y (or different packing density of resonators) overlap well with each other, revealing negligible interaction between adjacent resonators. This is because the electric field in an individual resonator is highly confined, as shown in Figures 2b and 3e,f.

For both the C-shape and the V-shape structures, we demonstrate that the thermal emission of the transmission line resonator arrays can be maximized by bending individual resonators. The arrays of the C-shape resonators are fabricated with different gap distances d, as shown in Figure 5a. As a comparison, the length, the width, and the thickness of all the C-shape resonators are fixed to be L = 1.4 μm, W = 200 nm, and H = 80 nm. Figure 5b shows the measured y-polarized emissivity spectra for different d, and the corresponding peak values are plotted in Figure 5c. The peak wavelength also agrees with the resonant wavelength of the fundamental Fabry−Perot type mode, and the trend of the peak height variation is consistent with our previous theoretical investigation. The fabricated C-shape resonators on the top of the reflective substrate represents a more general and complex example of the bended transmission line resonators in comparison with the standalone C-shape structures as shown in Figure 3c. Therefore, the curves in Figure 5c and Figure 3c follow the same trend (i.e., spectral emissivity first increases and then deceases as the increase of gap distance) but have different peak locations and line-shapes, which is attributed to the difference of the exact values of the dissipative and radiative mode losses (η_E, η_∞) between these two cases as well as the difference between the relative changes of the radiative mode loss when tuning the gap distance of these two different structures. At $d \sim$

DOI: 10.1021/acs.nanolett.6b03616
Nano Lett. 2017, 17, 666−672

400 nm, the emissivity peak approaches the blackbody radiation limit. For this optimized structure, we measure the emissivity spectra at different polarizations, as shown in Figure 5d. The *x*-polarized emissivity is almost zero at the resonant wavelength because the equivalent dipole moment of the C-shape transmission line resonator is polarized along the *y*-direction.

We also investigate the arrays of the V-shape resonators with different bending angles θ, as shown in Figure 6a. The length and the width of the V-shape transmission lines are fixed to be $L = 1\ \mu m$, $W = 0.13\ \mu m$, respectively. The thermal emissivity spectra and the corresponding peak heights at different θ are plotted in Figure 6b,c, respectively. The peak can also be maximized with a similar trend of the peak height variation in our theoretical investigation. Hence, bending the transmission line structures (i.e., tuning the radiative mode loss due to the modified dipole moment) serves as the other general principle to maximize the thermal emission of the transmission line resonator arrays.

As nanoscale building blocks, transmission line resonators, that is, cropped transmission lines with finite length, provide us a universal platform to construct macroscopic perfect and tunable thermal emitters. Rather than following the well-known metamaterial framework, we adopt the recently developed quasi-normal mode theory and experimentally demonstrate a general principle to maximize the thermal emission of nanoscale transmission line resonator arrays by tuning the dissipative and radiative mode losses of an individual transmission line resonator. Our experimental work in conjunction with the general theoretical framework therefore paves the way for tailoring the thermal emission from nanoscale resonators. This enables the development of various new technologies for thermal infrared light sources, thermal management, and infrared sensing and imaging.

Methods. *Quasi-Normal Mode Theory.* For an optical resonator thermal emitter with a predominant resonant mode, its thermal emission power density near the resonant frequency ω_0 equals $\phi(\omega) = L(\omega)\psi$, where $L(\omega) = 1/\{1 + (\mathrm{Re}[\omega_0] - \omega)^2/\mathrm{Im}[\omega_0]^2\}$ is the Lorentz line shape function with the peak at $\omega = \mathrm{Re}[\omega_0]$, and $\psi = \frac{\Theta}{2\pi}\eta_E\eta_\infty$ indicates the peak height.[15] The fractional mode losses η_E and η_∞ equal

$$\eta_E = \frac{D_E}{D_E + D_\infty}F$$

$$\eta_\infty = P - \eta_E \tag{5}$$

where

$$D_E = \int_V \mathrm{d}r^3 \frac{1}{2}\sigma|E_0(r)|^2$$

$$D_\infty = \int_{V'} \mathrm{d}r^2 \frac{1}{2}\mathrm{Re}[E_0(r) \times H_0^*(r)] \tag{6}$$

σ is the electric conductivity of the emitter, V' is an arbitrary auxiliary volume encompassing the entire emitter V. The imperfection factors F and P due to the non-Hermitian nature of the system are expressed as

$$F = \frac{\left|\int_{V'} \mathrm{d}r^3 \mathrm{Re}\left[\frac{\partial\omega\epsilon}{\partial\omega}(\mathrm{Re}[\omega_0])\right]|E_n(r)|^2 + \mu_0|H_0(r)|^2\right|}{|N|}$$

$$P = \frac{\mathrm{Re}\left[\frac{\int_V \mathrm{d}r^3\sigma E_0^2}{N}\right]}{\left\{\frac{\int_V \mathrm{d}r^3\sigma|E_0|^2}{|N|}\right\}} \leq 1 \tag{7}$$

By solving $[E_0, H_0]$, that is, the eigen-solution of the Maxwell equations, η_E and η_∞ can be calculated directly. The thermal emission peak value ψ is maximized when $\eta_E = \eta_\infty = \frac{P}{2}$. For the resonant emitters with quasi-static electric fields, $P \to 1$ and the ψ reaches the upper limit $\Theta/2\pi$.[15]

Sample Fabrication and Characterization. The sample fabrication begins with the sputtering of a 50 nm thick aluminum thin film as the metal ground plate on a SiO_2 thermal oxide wafer. Then a 150 nm thick aluminum oxide layer is sputtered on top of the aluminum, which serves as the dielectric spacer. The transmission line resonator arrays are fabricated by standard E-beam lithography techniques and subsequent lift-off process. The reflectivity of the samples is measured by using a FTIR spectrometer (Bruker IFS 66/s) combined with an infrared microscope (Bruker Hyperion 3000, with liquid nitrogen cooled MCT detector, KBr beam splitter, 15× Cassegrain objective lens with a numerical aperture of 0.4, and a 40 μm × 40 μm focusing spot size).

■ ASSOCIATED CONTENT

Supporting Information

The Supporting Information is available free of charge on the ACS Publications website at DOI: 10.1021/acs.nanolett.6b03616.

(i) Emissivity of the bare substrate; (ii) SEM image of the cross-section of the bare substrate; (iii) thermal emission power spectra of a straight transmission line resonator; (iv) emissivity spectra of the V-shape transmission line resonator arrays with different thickness; (v) angular power distribution of spectral thermal emission from a straight and a V-shape transmission line resonators at peak wavelengths (PDF)

■ AUTHOR INFORMATION

Corresponding Author

*E-mail: sshen1@cmu.edu.

ORCID

Sheng Shen: 0000-0002-9951-0814

Notes

The authors declare no competing financial interest.

■ ACKNOWLEDGMENTS

This work was supported by U.S. National Science Foundation (CBET-1253692).

■ REFERENCES

(1) Inoue, T.; De Zoysa, M.; Asano, T.; Noda, S. *Optica* **2015**, *2* (1), 27−35.

(2) Lenert, A.; Bierman, D. M.; Nam, Y.; Chan, W. R.; Celanović, I.; Soljačić, M.; Wang, E. N. *Nat. Nanotechnol.* **2014**, *9* (2), 126−130.

(3) Basu, S.; Zhang, Z. M.; Fu, C. J. *Int. J. Energy Res.* **2009**, *33* (April), 1203−1232.

(4) Raman, A. P.; Anoma, M. A.; Zhu, L.; Rephaeli, E.; Fan, S. *Nature* **2014**, *515*, 540.

(5) Otey, C. R.; Lau, W. T.; Fan, S. *Phys. Rev. Lett.* **2010**, *104* (15), 154301.

DOI: 10.1021/acs.nanolett.6b03616
Nano Lett. 2017, 17, 666−672

(6) Liu, B.; Liu, Y.; Shen, S. *Phys. Rev. B: Condens. Matter Mater. Phys.* **2014**, *90* (19), 195411.
(7) Liu, X.; Tyler, T.; Starr, T.; Starr, A. F.; Jokerst, N. M.; Padilla, W. J. *Phys. Rev. Lett.* **2011**, *107* (JULY), 4−7.
(8) Ghebrebrhan, M.; Bermel, P.; Yeng, Y. X.; Celanovic, I.; Soljačić, M.; Joannopoulos, J. D. *Phys. Rev. A: At., Mol., Opt. Phys.* **2011**, *83* (3), 033810.
(9) Schurig, D.; Mock, J. J.; Justice, B. J.; Cummer, S. a; Pendry, J. B.; Starr, a F.; Smith, D. R. *Science* **2006**, *314* (5801), 977−980.
(10) Landy, N. I.; Sajuyigbe, S.; Mock, J. J.; Smith, D. R.; Padilla, W. J. *Phys. Rev. Lett.* **2008**, *100* (20), 1−4.
(11) Sommerfeld, A. *Ann. Phys.* **1926**, *386* (25), 1135−1153.
(12) Mandviwala, T. A.; Lail, B. A.; Boreman, G. D. *Microw. Opt. Technol. Lett.* **2008**, *50* (5), 1232−1237.
(13) Schnell, M.; Alonso-González, P.; Arzubiaga, L.; Casanova, F.; Hueso, L. E.; Chuvilin, A.; Hillenbrand, R. *Nat. Photonics* **2011**, *5* (5), 283−287.
(14) Gacemi, D.; Mangeney, J.; Colombelli, R.; Degiron, A. *Sci. Rep.* **2013**, *3*, 1369.
(15) Liu, B.; Li, J.; Shen, S. Quasi-Normal Mode Theory for Thermal Radiation from Lossy and Dispersive Optical Resonators. 2016, arXiv:1509.00939. (accessed Nov 29, 2016).
(16) Fernandez-Cuesta, I.; Nielsen, R. B.; Boltasseva, A.; Borrisé, X.; Pérez-Murano, F.; Kristensen, A. *J. Vac. Sci. Technol. B Microelectron. Nanom. Struct.* **2007**, *25* (6), 2649.
(17) Sun, Y.; Yin, Y.; Mayers, B. T.; Herricks, T.; Xia, Y. *Chem. Mater.* **2002**, *14* (11), 4736−4745.
(18) Novotny, L.; Hecht, B. *Principle of Nano-Optics*, 2nd ed.; Cambridge University Press: Cambridge, U.K., 2012.
(19) Siegel, R. *Thermal Radiation Heat Transfer*, 4th ed.; Taylor & Francis: New York, 2001.
(20) Schuller, J. A.; Taubner, T.; Brongersma, M. L. *Nat. Photonics* **2009**, *3*, 658−661.
(21) Sauvan, C.; Hugonin, J. P.; Maksymov, I. S.; Lalanne, P. *Phys. Rev. Lett.* **2013**, *110* (23), 237401.
(22) Bai, Q.; Perrin, M.; Sauvan, C.; Hugonin, J.-P.; Lalanne, P. *Opt. Express* **2013**, *21* (22), 27371.
(23) Jackson, J. D. *Classical Electrodynamics*; Wiley: New York, 1998.
(24) Ikeda, K.; Miyazaki, H. T.; Kasaya, T.; Yamamoto, K.; Inoue, Y.; Fujimura, K.; Kanakugi, T.; Okada, M.; Hatade, K.; Kitagawa, S.; Ikeda, K.; Miyazaki, H. T.; Kasaya, T.; Yamamoto, K.; Inoue, Y.; Fujimura, K. *Appl. Phys. Lett.* **2008**, *92*, 021117.
(25) Inoue, T.; De Zoysa, M.; Asano, T.; Noda, S.; Inoue, T.; Zoysa, M.; De Asano, T.; Noda, S. *Appl. Phys. Lett.* **2013**, *102*, 191110.

DOI: 10.1021/acs.nanolett.6b03616
Nano Lett. 2017, 17, 666−672